ELSEVIER

Biophysical Chemistry 64 (1997) 127–137

Biophysical Chemistry

Kinetic analysis of a protein antigen–antibody interaction limited by mass transport on an optical biosensor

David G. Myszka [a,*,1], Thomas A. Morton [a,2], Michael L. Doyle [b], Irwin M. Chaiken [a,3]

[a] *Department of Molecular Immunology, SmithKline Beecham Pharmaceuticals, King of Prussia, PA 19406, USA*
[b] *Department of Macromolecular Sciences, SmithKline Beecham Pharmaceuticals, King of Prussia, PA 19406, USA*

Received 10 July 1996; accepted 23 August 1996

Abstract

Using BIAcore™ technology, we determined the rate constants for a protein antigen–antibody interaction that was mass transport limited on the optical biosensor. The antigen consisted of a soluble form of the human T-cell receptor CD4 (two amino terminal domains, D1D2) and the antibody was an anti-CD4 monoclonal from monkey engineered with the constant domains from human IgG1. High quality response data were obtained for this interaction by orienting the attachment of the antibody on the sensor surface and correcting for instrument artifacts with control experiments. Using numerical integration and global fitting, we demonstrate that a mass transport limited reaction was the only model of those tested that described well D1D2 binding to three different surface densities of the antibody. Statistical profiling techniques showed that the error space and correlation for the parameters in the non-linear model were essentially linear, but only when the model was simultaneously fitted to data from multiple surface densities. The "on" and "off" rate constants (1.2×10^{-6} M^{-1} s^{-1} and 2.9×10^{-4} s^{-1}) determined from the kinetic analysis predict an equilibrium dissociation constant ($K_D = 0.24 \pm 0.01$ nM) that agrees with the value measured in solution by titration calorimetry ($K_D = 0.2 \pm 0.1$ nM). The results indicate that, although the D1D2–antibody reaction is partially controlled by mass transport on the optical biosensor, by optimizing the experimental design and analyzing data from multiple surface densities it is possible to determine accurate estimates of the intrinsic equilibrium and kinetic rate constants.

Keywords: Surface plasmon resonance; BIAcore; Biosensor; Mass transport; Kinetics; Protein–protein interaction

1. List of symbols and abbreviations

Anti-Fc1	Human IgG Fc1-specific antibody
D1D2	truncated human CD4 receptor
B_{max}	maximum surface capacity
EDC	*N*-ethyl-*N'*-(3-diethylaminopropyl)carbodiimide
k_m	mass transport coefficient
k_{off}	"off" rate constant

* Corresponding author. Tel.: (801)-585-5358; fax.: (801)-585-3833; e-mail: dmyszka@genetics.utah.edu.

[1] Present address: Department of Oncological Sciences, Huntsman Cancer Institute, University of Utah, EIHG Building 533, Rm. 7145, Salt Lake City, UT 84112, USA.

[2] Present address: Division of Biochemistry and Molecular Biology, John Curtin School of Medical Research, Australian National University, Canberra, ACT 0200, Australia.

[3] Present address: Rheumatology Division, University of Pennsylvania School of Medicine, Philadelphia, PA 19104, USA.

PII S0301-4622(96)02230-2

k_{on}	"on" rate constant
K_D	equilibrium dissociation constant
mAb	monoclonal antibody
NHS	*N*-hydroxysuccinimide
RU	resonance units

2. Introduction

Optical biosensors can be used to monitor the interactions of macromolecules in real time, potentially providing access to the chemical rate constants that govern their binding reactions. A major advantage of these instruments is that the reactants do not need to be labeled with radioactive or spectroscopic probes. On the other hand, one of the reactants must be attached to the sensor surface. This in turn places limitations on the ability to accurately determine rate constants for fast binding reactions, because the reactant in solution must first be transported by diffusion to the surface in order to bind to its immobilized partner [1–4].

BIAcore™, an optical biosensor from BIAcore Inc., uses surface plasmon resonance technology to monitor the refractive index change as molecules absorb onto or dissipate from the sensor surface during a reaction [5,6]. Most interactions reported have been performed with the ligand immobilized onto a carboxymethyl dextran matrix that coats the sensor surface. This matrix provides a hydrophilic and freely mobile environment that is conducive to measuring protein interactions [7]. The analyte is passed over the sensor surface using a micro flow cell that has been optimized to reduce mass transport effects [3]. These effects can be further minimized by increasing the flow rate and lowering the surface capacity [4,8], but for many reactions the binding rates are too fast to be eliminated completely. The only way to accurately determine the rate constants for these types of reactions is to analyze the data with a model that includes mass transport in the overall reaction. Successfully fitting complex reaction mechanisms to biosensor data requires the implementation of global fitting. This provides a stringent test of the proposed binding mechanism but also places high demands on the quality of the sensor data [9].

In this paper we demonstrate the ability to determine the rate constants for a protein antigen–antibody reaction that is mass transport limited on BIAcore™. The antigen is a truncated version of the human T-cell receptor CD4 containing the two amino terminal extracellular domains, D1D2 [10]. CD4 plays a critical role in T-cell activation and differentiation during the immune response, and the X-ray crystal structure has been solved for the D1D2 extracellular domains [11,12]. The antibody is a chimera made by the fusing of the antigen-binding variable domains from a monkey anti-human-CD4 mAb with constant domains from a human IgG1 mAb and is referred to as mAb CE9.1 [13,14].

We designed the D1D2–mAb CE9.1 biosensor assay with a number of experimental considerations. First, the mAb was captured on the sensor surface using an immobilized anti-Fc1 IgG surface. This created a homogeneous reaction surface of mAb CE9.1 and allowed us to monitor a monovalent interaction with the D1D2 in solution. To improve the quality of the response data, we also employed low surface densities of the mAb, injected D1D2 at high flow rates, and performed control experiments to correct for refractive index changes and nonspecific binding. We collected D1D2 binding data across three different surface densities of mAb CE9.1 and tested different possible reaction mechanisms using numerical integration and global curve fitting. We show that by optimizing the experimental design and applying robust analysis procedures, it is possible to accurately determine the kinetic rate constants for interactions that are partially limited by mass transport on the biosensor.

3. Experimental procedures

3.1. Materials

The truncated soluble form of the human T-cell receptor CD4 (extracellular domains D1D2) was produced as a secreted protein in transfected Chinese hamster ovary cells, and purified with a combination of ion-exchange and size-exclusion chromatography [10]. The mAb CE9.1 is a PRIMATIZED™ (monkey–human chimera) mAb [14] which was expressed in Chinese hamster ovary cell lines with hollow fiber technology at IDEC Pharmaceuticals

(San Diego, CA) and purified on a Prosep A column (Bioprocessing Ltd.) [10]. An IgG specific for the human Fc1 (anti-Fc1) was purchased from Pierce Co. (Rockford, IL). All proteins were more than 98% pure by reducing SDS-PAGE densitometry. BIAcore, CM5 certified sensor chips, NHS/EDC coupling reagents, ethanolamine, and P20 were from BIAcore Inc., (Uppsala, Sweden).

3.2. Biosensor experiments

Three anti-Fc1 surfaces were created using the standard amine coupling procedure described previously [15]. Each carboxymethyl dextran surface was activated with a 7 min injection of a mixture of NHS/EDC (each 0.1 M in water). Anti-Fc1 was coupled at different densities (4600, 2000, and 570 RU) by exposing each surface to a 10 mg ml^{-1} sample in 10 mM acetate, pH 5.0, for 300, 60, or 15 s at a flow rate of 5 $\mu l\ min^{-1}$. After the coupling step, the remaining activated groups were blocked with a 7 min wash of 1 M ethanolamine, pH 8.2, followed by several 10 s washes with 100 mM phosphoric acid to remove non-covalently bound protein.

All biosensor experiments were performed in buffer containing 150 mM NaCl, 10 mM HEPES, 3.4 mM EDTA, and 0.005% P20, pH 7.4 at 25°C. The effect of flow rate on the binding response was tested using a 3000 RU mAb surface and a D1D2 concentration of 75 nM, injected at a flow rate of 1, 5, 25, and 125 $\mu l\ min^{-1}$. To generate the kinetic binding data, mAb CE9.1 was first captured on the anti-Fc1 surface by injecting 25 μl at 100 nM concentration at a flow rate of 5 $\mu l\ min^{-1}$. The flow rate was changed to 25 $\mu l\ min^{-1}$ and the surface was washed for 10 min with running buffer prior to injecting a 25 μl sample of D1D2. D1D2 dissociation was then monitored for 600 s, after which time the remaining D1D2–mAb CE9.1 complex was removed from the anti-Fc1 surface with a 5 μl injection of 100 mM phosphoric acid. These binding experiments were repeated for D1D2 concentrations of 0, 8.3, 25, 75, 225, and 675 nM, over surfaces containing 1400, 500, and 150 RU of the captured mAb. The same D1D2 samples were also injected over each anti-Fc1 surface in the absence of captured mAb as controls for refractive index change and non-specific binding.

Biosensor data were prepared for analysis by subtracting the average of the response recorded over 20 s prior to injecting the D1D2 and adjusting the time of each injection to zero. To correct for the refractive index change and non-specific binding, the response obtained from each D1D2 sample injected over the surface in the absence of the mAb was subtracted from the corresponding D1D2–mAb binding data.

3.3. Modeling of sensor data

Several binding mechanisms were tested against the D1D2–mAb interaction data. In each reaction below, A represents the injected D1D2, except in the mass transport limited reaction (Eq. (2)), in which it is represented by A_o.

Simple bimolecular

$$A + B \underset{k_{off}}{\overset{k_{on}}{\rightleftharpoons}} AB \tag{1}$$

Mass transport limited

$$A_o \underset{k_m}{\overset{k_m}{\rightleftharpoons}} A + B \underset{k_{off}}{\overset{k_{on}}{\rightleftharpoons}} AB \tag{2}$$

Two-state conformational change

$$A + B \underset{k_{off}}{\overset{k_{on}}{\rightleftharpoons}} AB \underset{k_{-2}}{\overset{k_2}{\rightleftharpoons}} (AB)^* \tag{3}$$

Three-state conformational change

$$A + B \underset{k_{off}}{\overset{k_{on}}{\rightleftharpoons}} AB \underset{k_{2}}{\overset{k_2}{\rightleftharpoons}} (AB)^* \underset{k_{-3}}{\overset{k_3}{\rightleftharpoons}} (AB)^{**} \tag{4}$$

Surface heterogeneity

$$A + \begin{array}{l} B \underset{k_{off1}}{\overset{k_{on1}}{\rightleftharpoons}} AB \\ B^* \underset{k_{off2}}{\overset{k_{on2}}{\rightleftharpoons}} AB^* \end{array} \tag{5}$$

The concentrations of the injected D1D2 samples were held constant during the association phase (0–

59.8 s) and set to zero at the start of the dissociation phase (60–600 s). In each reaction, B or B* represents the CD4 binding sites on the immobilized mAb that are assumed to interact with D1D2 independently. The symbols above and below the arrows represent the rate constants for each reaction step.

3.4. Curve fitting and statistical analysis

Modeled data for each binding mechanism were generated by numerical integration of their differential rate equations using the Bader and Deuflhard semi-implicit extrapolation method [16]. The concentrations of surface bound species (AB, AB*, (AB)* or AB**) and the maximum surface capacity, B_{max}, were modeled in resonance units. The data collected from each sensor surface required a separate B_{max}, while the rate constants for the reactions were applied simultaneously to data from multiple surface densities. The total number of unknown parameters used during any analysis depended on the number of data sets being fitted and the reaction mechanism being tested. To perform non-linear least-squares analysis, the values for the unknown parameters were adjusted by the Levenberg–Marquardt method [16] to minimize the difference between the modeled and real data. To ensure that a true minimum had been found, the fitting process was repeated 100 times with different starting values. The minimization routine was stopped when the fractional change in the sum of squares went below 0.001. The computational routines used in this study were similar to those previously reported [9] and were run on a personal computer with a 100 MHz processor.

Statistical profiling was used to derive accurate estimates of the variance and correlation for parameters within the non-linear models [17]. Profiles for each parameter were generated by varying one parameter around its best fit value and solving for the conditional sum of squares. Profile t plots were created by shifting and scaling these parameter values to Studentized values, and converting the profile sum of squares to profile t values [18]. Profile trace plots contain the pairwise plots of the trace vector versus the profiled parameter. These data were combined with information from the profile t plots, to determine accurate contour levels at 68, 90, and 95% confidence intervals shown on the profile trace plots.

4. Results

4.1. Flow-rate analysis

A straight line in the association phase is often the first indication that a reaction may be mass transport limited on the biosensor. One easy way to test for the presence of this effect is to alter the flow rate [4]. Increasing the flow rate delivers analyte to the immobilized ligand at a faster rate but it will not change the interaction kinetics [4,8]. Fig. 1 shows that altering the flow rate from 1 to 125 μl min^{-1} significantly increased the binding rate for D1D2 to the mAb surface, indicating that under these conditions, the reaction is partially limited by mass transport. Due to restrictions in the injection volume (about 25 μl), we chose to run the kinetic experiments at a flow rate of 25 μl min^{-1}. This would lessen the effects of mass transport, yet allow sufficient time in the association phase for the higher concentrations of D1D2 to saturate the mAb CE9.1 surface. The higher flow rate also serves to minimize dilution of the sample plug.

4.2. Kinetic binding data

Fig. 2 shows an example of the raw binding data generated to resolve the kinetics of the D1D2–mAb interaction. We monitored a monovalent interaction and created a homogeneous reacting surface by attaching the CD4 mAb to the dextran layer using an immobilized IgG specific for human Fc1. The initial large binding response represents mAb CE9.1 being

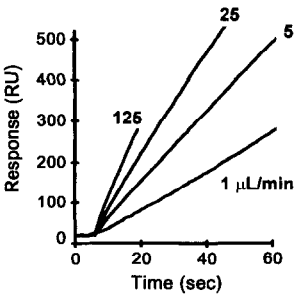

Fig. 1. The effects of flow rate on the D1D2 binding response. D1D2 was injected at a concentration of 75 nM over a 3000 RU mAb CE9.1 surface at flow rates of 1, 5, 25 and 125 μl min^{-1}, as labeled.

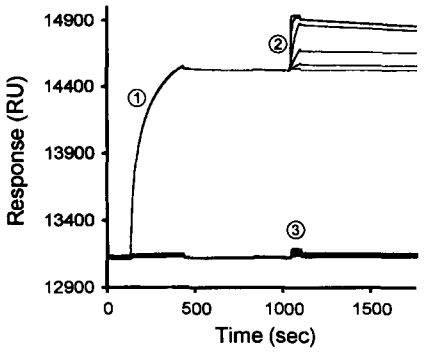

Fig. 2. Raw binding data collected for the biosensor D1D2–mAb interaction. The binding response at region (1) is an overlay of six repeated mAb CE9.1 injections over the 4600 RU anti-Fc1 surface. The responses at region (2) are from the D1D2 injections at concentrations of 0, 8.3, 25, 75, 225 and 675 nM. Region (3) shows the response for the same D1D2 samples injected over the anti-Fc1 surface without captured mAb CE9.1.

captured by the anti-Fc1 surface. This line is an overlay of six replicate injections of the mAb and shows that the anti-Fc1 surface captures the same amount of mAb each time, indicating that the surface is very stable under the phosphate regeneration conditions. The high reproducibility of this procedure allowed direct comparison of the binding responses for a series of D1D2 concentrations starting with essentially identical mAb CE9.1 surfaces. The anti-Fc1–mAb CE9.1 complex itself was also very stable, and over the time frame in which we monitored the reaction with D1D2, the decay of mAb CE9.1 was negligible. The raw D1D2 binding data, however, does contain a refractive index change in the association phase and a small amount of non-specific binding. To correct for these system artifacts, control experiments were run with the same D1D2 samples injected over the same anti-Fc1 surface in the absence of mAb, also shown in Fig. 2. These control responses were subtracted from the D1D2–mAb binding data to yield the corrected sensorgrams shown in Fig. 3A for D1D2 binding to three different surface densities of mAb CE9.1 (1400, 500 and 150 RU).

To better visualize the shapes of the progress curves and the relationships between the data sets, the sensorgram overlays from the different density surfaces were rescaled as shown in Fig. 3B. The two highest concentrations of D1D2 (675 and 225 nM) saturated each surface and decayed at the same rate, providing information about the surface capacity (see Section 4.4 below). If the D1D2–mAb interaction was a simple bimolecular reaction, the rescaled responses should look identical regardless of the surface density. However, the binding responses appeared to increase as the mAb surface density was lowered. In other words, the responses from the lower density surfaces were approaching equilibrium faster than those recorded from the higher density surface. Unfortunately, due to restrictions in the injection volume, only the two highest concentrations of D1D2 were given enough time in the association phase to reach equilibrium. Therefore, we were unable to determine the affinity for the interaction from equilibrium analysis, which would be insensitive to the mass transport effect, and instead we interpreted the reaction kinetics by direct curve fitting.

4.3. Comparison of kinetic binding mechanisms

We tested different binding mechanisms for the D1D2–mAb interaction by simultaneously fitting the association and dissociation data from the three mAb surfaces. The best fit of a simple bimolecular reaction (see Eq. (1), five parameters) is shown in Fig. 4A. A visual comparison of the overlay plots for the

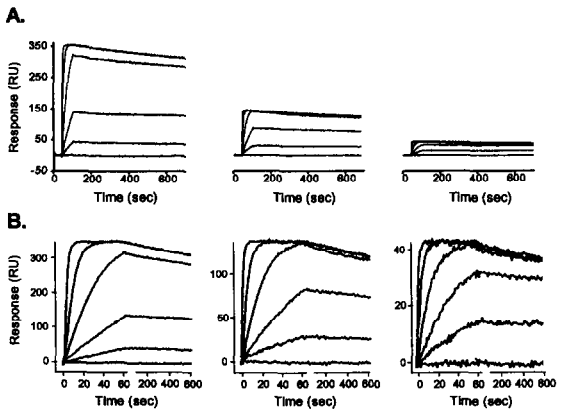

Fig. 3. The corrected D1D2–mAb binding responses. (A) D1D2 at concentrations of 0, 8.3, 25, 75, 225 and 675 nM were injected over three surfaces with different amounts of captured mAb CE9.1 (1400, 500, and 150 RU). (B) The same binding responses as in the (A) plots were rescaled to better visualize and compare the responses.

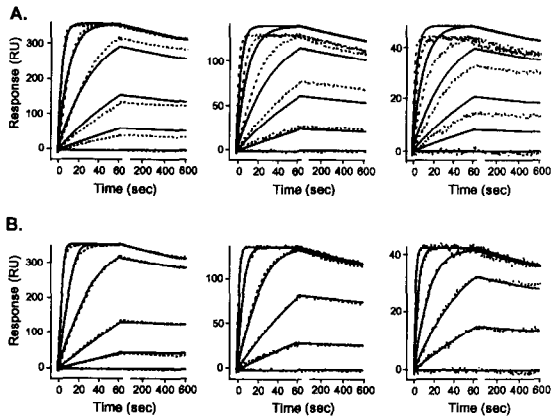

Fig. 4. Global fitting to the D1D2 binding data (broken lines). (A) Best fit to a simple bimolecular interaction model (Eq. (1)) (solid lines). The standard deviation of the residuals was 35 RU. (B) Best fit to a mass transport limited model (Eq. (2)) (solid lines). The standard deviation of the residuals was 2.2 RU.

model versus the data shows that this reaction does not describe the data very well, and given the high standard deviation in the residuals of 35 RU, this is clearly a poor fit. This model also failed to describe the reaction when fitted to data from each surface independently (not shown). We attempted to fit these data using more complex reaction models including a two-state conformational change (Eq. (3), seven parameters), a three-state conformational change (Eq. (4), nine parameters), and a surface heterogeneity reaction (Eq. (5), ten parameters). Although each of these models contained additional floating parameters, they all failed to improve the quality of the fit versus a simple bimolecular reaction. In contrast, a bimolecular reaction incorporating mass transport limitations [4,8] (Eq. (2), six parameters) adequately described the data, as shown in the overlay plot in Fig. 4B. The standard deviation in the residuals of this fit was 2.2 RU. This is close to the short term random noise of the BIAcore which is around 1 RU [19]. A slightly improved fit was obtained when the mass transport model was fitted to data from only one surface at a time (not shown), and while the values for the parameters did not significantly change, their standard deviations increased. This made the confidence intervals and correlations for some of the parameters appear highly non-linear as demonstrated below.

4.4. Parameter confidence intervals and correlation

Profile t and trace plots were used to visualize the error space and correlation for the parameters from the mass transport limited model. A profile t plot is created by centering the best fit parameter value at zero and rescaling the error space, which is normally parabolic for linear models, to conform to a line with unit slope [17]. Therefore, deviations from a straight line at a 45° angle are an indication of non-linearity in the parameter's error space. The profile plots for the six parameters from the mass transport bimolecular reaction (B_{max1}, B_{max2}, B_{max3}, k_m, k_{on}, and k_{off}) are shown on the diagonal of the matrix in Fig. 5. All these plots are nearly straight lines with unit slope, indicating that the error space around each parameter is symmetrical and therefore, the parameter confidence intervals are essentially linear.

The correlations between the parameters were visualized using profile trace plots [18], which are displayed off the diagonal of the matrix in Fig. 5. The contour levels on these plots show the joint 68, 90, and 95% confidence regions for each set of parameters. For a linear model, each contour plot would be a perfect ellipse; and the narrower the ellipse, the higher the correlation. Also, the direction of the main elliptical axis determines whether the parameters are positively or negatively correlated. Since the mass transport model had six parameters, it required a total of 15 trace plots to generate all the cross correlations. All the contour plots were nearly perfect ellipses, indicating that the correlations between all the parameters were essentially linear. Some of the trace plots, as for B_{max2} vs. B_{max3} and B_{max1} vs. k_m showed nearly circular contour levels, indicating no correlation between these parameters. In fact, out of all the trace plots, the only one that contained significantly narrow contour levels was for the parameters k_m vs. k_{on}. This indicates that these parameters are more highly correlated and the negative slope shows that the correlation is negative.

To demonstrate the benefits of simultaneously fitting data from multiple surface densities, Fig. 6 shows the profile plots for the mass transport model fitted to D1D2 binding data from only one mAb surface. The profile plots for parameters B_{max2} and k_{off} were still linear and their trace plots (B_{max2} vs. k_{off}) were elliptical, but the profile and trace plots

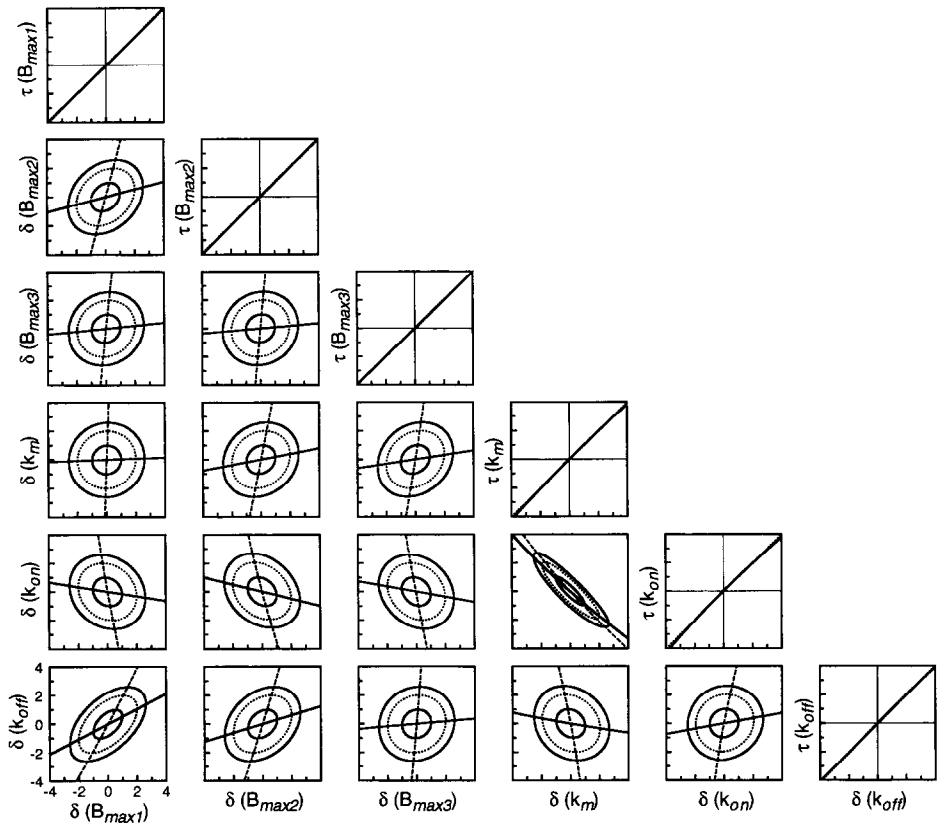

Fig. 5. Profile plots for the parameters in the mass transport model (Eq. (2)) globally fit to the D1D2 binding data from three surface densities of mAb CE9.1. Profile t plots are shown on the diagonal of the matrix (solid line) and include a linear reference line (broken line at 45°). In the profile trace plots (off the diagonal of the matrix) the solid and broken intersecting lines are the profile traces. The solid and broken closed lines correspond to 68, 90 and 95% joint likelihood regions. The scales shown in the lower left-hand corner are applicable to all the plots in the figure.

involving the parameters k_m and k_{on} appeared non-linear, indicating that their error spaces and correlations were now non-linear.

Because all the parameters for the mass transport limited model when fitted to the binding data from multiple surface densities were essentially linear, we can report their standard deviations and correlations using the linear approximation statistics directly from the covariance matrix [18], as shown in Table 1. The standard deviations for all the parameter values were very low (averaging around 1%). All the parameter correlations were also very low except for k_m vs. k_{on} (−0.90), as was shown by the profile trace plots (Fig. 5). It was not unexpected that these parameters would be correlated due to their relationship in the model, yet computationally this level of correlation is not high enough to justify concern, as unique estimates for the parameters were found.

The maximum capacity of each surface (B_{max1}, B_{max2}, B_{max3}) was used to determine the binding stoichiometry of the mAb. Based on the amount of mAb CE9.1 captured and the molecular mass of each protein, the antibody surfaces averaged a binding stoichiometry of 1:1.98 D1D2 molecules. This is consistent with the antibody having two recognition sites for D1D2, and shows that the specific activities of these surfaces were very high. The value determined for the mass transport coefficient (6.4×10^{-6} m s^{-1}) is approximately two times slower than the value predicted for D1D2 diffusing through the unstirred solvent layer alone. The mean mass transport coefficient in rectangular flow cells was approxi-

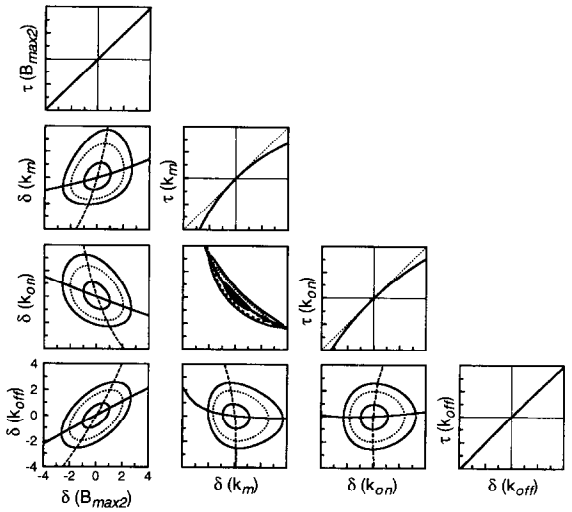

Fig. 6. Profile plots for the parameters in the mass transport model (Eq. (2)) fit to the D1D2 binding data from the 500 RU mAb CE9.1 surface only. Profile t plots are shown on the diagonal of the matrix (solid line) and include a linear reference line (broken line at 45°). In the profile trace plots (off the diagonal of the matrix) the solid and broken intersecting lines are the profile traces. The solid and broken closed lines correspond to 68, 90 and 95% joint likelihood regions. The scales shown in the lower left-hand corner are applicable to all the plots in the figure.

mated based on the mass of the analyte, the dimensions of the flow cell, and the flow rate [3,4]. However, the calculation ignores any contribution of the dextran matrix, which is likely to slow the transport rate due to increased viscosity. The "on" and "off" rate constants were determined as 1.2×10^6 M^{-1} s^{-1} and 2.9×10^{-4} s^{-1}, respectively. This "on" rate is sufficiently fast that the D1D2–mAb interaction would be predicted to be influenced by mass transport on the biosensor [4]. At equilibrium, the transport reaction can be ignored and the resulting rate constants from the kinetic analysis can be used to calculate an equilibrium dissociation constant (k_{off}/k_{on}) of 0.24 ± 0.01 nM for the D1D2–mAb CE9.1 interaction.

Table 1
Parameter estimates, standard deviations and correlation coefficients from the global fit of the mass transport limited model to the D1D2–mAb binding data

Parameter	Estimate	Standard Deviation	Units
B_{max1}	357	±0.5	RU
B_{max2}	132	±0.4	RU
B_{max3}	43	±0.3	RU
k_m	6.4×10^{-6}	$\pm 7 \times 10^{-8}$	$m\ s^{-1}$
k_{on}	1.2×10^6	$\pm 2 \times 10^4$	$M^{-1}\ s^{-1}$
k_{off}	2.9×10^{-4}	$\pm 7 \times 10^{-6}$	s^{-1}

Correlation coefficients

	B_{max1}	B_{max2}	B_{max3}	k_m	k_{on}
B_{max2}	0.26				
B_{max3}	0.10	0.09			
k_m	0.03	0.19	0.16		
k_{on}	−0.15	−0.25	−0.18	−0.90	
k_{off}	0.53	0.31	0.09	−0.19	0.19

5. Discussion

Accurate determination of kinetic rate constants for reactions limited by mass transport on the biosensor benefits greatly from global analysis of data sets representing multiple surface densities. Global analysis places a high demand on the quality of the sensor data and accuracy of the fitting model. Therefore, we designed the biosensor assay for the D1D2–mAb interaction with a number of considerations aimed at optimizing the quality of the experimental data. Since the antibody has two antigen binding sites, we attached it to the sensor surface in order to monitor a monovalent interaction with soluble D1D2. Several methods were available to attach the mAb onto the dextran matrix [20]. We chose to capture mAb CE9.1 with an immobilized anti-Fc1 IgG antibody for several reasons. First, the anti-Fc1 surface enabled us to orient mAb CE9.1 to create a homogeneous surface. Second, it was easy to control the density of mAb CE9.1 by capturing more or less of it. Third, the mAb CE9.1–anti-Fc1 interaction was very stable and there was negligible decay of the complex over the time period in which we monitored the interactions with D1D2. Fourth, the anti-Fc1 surface itself was very sturdy and could be fully regenerated without loss of mAb CE9.1 binding capacity. Finally, by monitoring the interaction of D1D2 in the absence of captured mAb CE9.1, we could run control experiments for refractive index change and non-specific binding directly on the same flow cell. This information was used to remove these artifacts from the

response data, generating sensorgrams that could be described by fewer parameters during curve fitting.

We also characterized the D1D2–mAb CE9.1 interaction by making measurements over a one-hundredfold concentration range of D1D2 and across three different surface densities of the mAb. Comparison of the rescaled sensorgram overlays revealed that the apparent binding rate was faster on the lower density surfaces. Lowering the surface capacity lowers the flux of analyte from within the unstirred layer and reduces the effects of mass transport [3,4,8]. Thus, data from the lower density surfaces contain more accurate information about the kinetic rate constants even though the signal-to-noise ratio is lower. The lowest density surface had a maximum capacity of around 40 RU, which still yielded reliable binding responses. The maximum binding capacity of each surface indicated that the captured mAb CE9.1 was highly active and bound stoichiometric amounts of D1D2. This verifies that the dextran environment did not occlude any of the D1D2 binding sites.

To determine the kinetics of the D1D2–mAb CE9.1 interaction, we tested a number of possible binding mechanisms using numerical integration and global fitting. Numerical integration allowed us to use models for which we do not have analytical solutions to the integrated rate equations. Globally fitting these models to all the binding data provided a stringent test for each proposed mechanism. A simple bimolecular reaction (Eq. (1)) failed to describe the D1D2–mAb binding responses. Interestingly, models for a two-step (Eq. (3)) or three-step (Eq. (4)) conformational change reaction and surface heterogeneity (Eq. (5)), which have increased numbers of floating parameters, all failed to improve the quality of the fit when compared to a simple bimolecular reaction. A bimolecular reaction limited by mass transport (Eq. (2)) was the only mechanism of those tested that accurately described the data, and contained only one additional parameter. The residual standard deviation was about 2 RU, which is close to the short-term random noise of the BIAcore instrument of about 1 RU [19]. However, the short-term noise does not take into consideration other sources of experimental error. Deviations introduced by sample dilution, machine drift, variability in the amount of mAb CE9.1 captured between experiments and protein stability, are also expected to contribute to the total experimental noise in the system.

The mass transport coefficient (k_m), which describes diffusion of D1D2 to and from the antibody sites, was found to be within a factor of two of the theoretical value. However, the theoretical value is based on diffusion through solvent alone and ignores any contribution of the dextran matrix, which is likely to slow the transport rate due to increased viscosity. Nevertheless, the observation that a single value for this parameter was necessary and sufficient to describe the binding responses recorded over a one-hundredfold concentration range of D1D2 and across three different surface densities of the antibody lends strong support for the mass transport limited model used.

Further support for application of the mass transport model for the D1D2–mAb CE9.1 case comes from a comparison of the affinity for the D1D2–mAb interaction calculated from kinetic "on" and "off" rates versus the affinity measured independently by solution titration calorimetry. The equilibrium dissociation constant calculated from the ratio of the "off" and "on" rate constants in Table 1 is equal to 0.24 ± 0.01 nM. This value is in excellent agreement with the value of 0.2 ± 0.1 nM measured in solution by isothermal titration calorimetry under the same solution conditions as in the present study [21].

The statistical confidence in the parameter estimates for the mass transport limited model were also examined. Because the model is based on non-linear rate equations, we could not rely on the values determined from the non-linear regression analysis, since they are based on linear assumptions [17]. A simple way to avoid linear-approximation summaries and to interpret accurate confidence regions for parameter estimates from non-linear models is to use profiling [18]. Our profiling analysis showed that, although the mass transport limited model was formally non-linear, the parameters were behaving as though they were linear. We showed that this was afforded by globally fitting data from multiple surface densities. In contrast, the parameters were non-linear when the model was fitted to data from only a single surface. The binding responses from the highest density surface contain more information about the mass transport coefficient, while the responses

from the lowest density surface had more information about the intrinsic binding rate constants. By analyzing data from multiple surfaces simultaneously, there was enough information to accurately determine values for each of the parameters in the model. The behavior of parameter estimates in non-linear models is a very complex function of how the equation is formulated, the way the parameters are expressed, the quality and amount of data, and even the parameter values themselves [18]. Therefore, it is necessary to assess parameter statistical behavior with each new data set and model that is tested. Fortunately, profile plots are an easy way to compare parameters both within and between data sets. If the parameters are found to be non-linear, then accurate upper and lower confidence intervals can be interpreted directly from the profile plots [18]. In the present case, the parameters were linear when the whole data set was globally analyzed, so we could quote the linear approximation statistics with assurance.

The present study demonstrates that incorporation of a mass transport step into the overall kinetic scheme for the interaction of soluble T-cell receptor CD4 with immobilized anti-CD4 mAb permits accurate estimates of the intrinsic chemical rate constants. The magnitude of the "on" rate constant, 1.2×10^6 M^{-1} s^{-1}, is tenfold larger than can be measured directly as a simple bimolecular process on a BIAcore biosensor. Even so, in order to achieve the present results, it was necessary to optimize considerably the experimental approach and to globally analyze data sets from multiple surface densities of the antibody. Recently, a macromolecular interaction measured on the sensor was shown to be described by a simple bimolecular interaction model [22], but the majority of the reported reactions appear more complex than expected. Different reasons have been invoked to describe these deviations, including heterogeneity of reactants, mutivalency, aggregation, non-specific binding, molecular crowding, allosteric interactions, multiple state reactions, and mass transport limitations. It is clear that many of these deviations can be minimized, eliminated, or corrected for by improvements in experimental design. Yet, there are likely to be interactions that follow complex reaction schemes whose resolution will greatly benefit through the application of global analysis.

Acknowledgements

We thank Preston Hensley from SmithKline Beecham for his discussions on error space analysis. The PRIMATIZED™ mAb CE9.1 used in this study was produced by IDEC Pharmaceuticals Corporation, San Diego, CA.

References

[1] M.J. Eddowes, Biosensors, 3 (1987) 1–15.
[2] R.W. Glaser, Anal. Biochem., 213 (1993) 152–161.
[3] S. Sjölander and C. Urbaniczky, Anal. Chem., 63 (1991) 2338–2345.
[4] R. Karlsson, H. Roos, L. Fägerstam and B. Persson, Methods: Companion to Methods in Enzymol., 6 (1994) 99–110.
[5] S. Löfås, M. Malmqvist, I. Ronnberg, E. Stenberg, B. Liedberg and I. Lundström, Sensors Actuators, B5 (1991) 79–84.
[6] U. Jönsson, L. Fägerstam, B. Ivarsson, B. Johnsson, R. Karlsson, K. Lundh, S. Löfås, B. Persson, H. Roos, I. Rönnberg, S. Sjölander, E. Stenberg, R. Ståhlberg, C. Urbaniczky, H. Östlin and M. Malmqvist, Biotechniques, 93 (1991) 620–627.
[7] S. Löfås and B. Johnsson, J. Chem. Soc., Chem. Commun., 21 (1990) 1526–1528.
[8] R.J. Fischer, M. Fivash, J. Casas-Finet, S. Bladen and K.L. McNitt, Methods: Companion to Methods in Enzymol., 6 (1994) 121–133.
[9] T.A. Morton, D.G. Myszka and I.M. Chaiken, Anal. Biochem., 227 (1995) 176–185.
[10] J. Arthos, K.C. Deen, M.A. Chaikin, J.A. Fornwald, G. Sathe, Q.J. Sattentau, P.R. Clapham, R.A. Weiss, J.S. McDougal, C. Pietropaolo, R. Axel, A. Truneh, P.J. Maddon and R.W. Sweet, Cell, 57 (1989) 469–481.
[11] T.P.J. Garrett, J. Wang, Y. Yan, J. Liu and S.C. Harrison, J. Mol. Biol., 234 (1993) 763–778.
[12] S.-E. Ryu, A. Truneh, R.W. Sweet and W.A. Hendrickson, Structure, 2 (1994) 1705–1729.
[13] M.L. Doyle, M.B. Brigham-Burke, I.S. Brooks, M.N. Blackburn, T.M. Smith, T. Sokoloski, R. Newman, M. Reff, R.M. Sweet, A. Truneh, P. Hensley and D.J. O'Shannessy, in preparation.
[14] R.A. Newman, J. Alberts, D. Anderson, C. Heard, F. Norton, R. Raab, M. Reff, S. Shuey and N. Hanna, Bio/Technology, 10 (1992) 1455–1460.
[15] B. Johnsson, S. Löfås and G. Lindquist, Anal. Biochem., 198 (1991) 268–277.
[16] W.H. Press, S.A. Teukolsky, W.T. Vetterling and B.P. Flannery, in Numerical Recipes in C, Cambridge University Press, Cambridge, 1992.

[17] D.M. Bates and D.G. Watts, Chemometrics Intelligent Lab. Syst., 10 (1991) 107–116.
[18] D.G. Watts, Can. J. Chem. Eng., 72 (1994) 701–710.
[19] BIAcore System Manual.
[20] B. Johnsson, L. Fagerstam, H. Nilshans and B. Persson, J. Mol. Recog., 8 (1995) 125–131.
[21] M.L. Doyle, D.G. Myszka and I. Chaiken, J. Mol. Recog., 9 (1996) 65–74.
[22] L.D. Rodin and D.G. Myszka, Biochem. Biophys. Res. Commun., 225 (1996) 1073–1077.